

Communication

Manipulating Topological Domain Boundaries in the Single-layer Quantum Spin Hall Insulator $1T'-WSe_2$

Zahra Pedramrazi, Charlotte Herbig, Artem Pulkin, Shujie Tang, Madeleine Phillips, Dillon Wong, Hyejin Ryu, Michele Pizzochero, Yi Chen, Eugene J. Mele, Feng Wang, Zhi-Xun Shen, Sung-Kwan Mo, Oleg V. Yazyev, and Michael F. Crommie

Nano Lett., **Just Accepted Manuscript** • DOI: 10.1021/acs.nanolett.9b02157 • Publication Date (Web): 22 Jul 2019

Downloaded from pubs.acs.org on July 22, 2019

Just Accepted

“Just Accepted” manuscripts have been peer-reviewed and accepted for publication. They are posted online prior to technical editing, formatting for publication and author proofing. The American Chemical Society provides “Just Accepted” as a service to the research community to expedite the dissemination of scientific material as soon as possible after acceptance. “Just Accepted” manuscripts appear in full in PDF format accompanied by an HTML abstract. “Just Accepted” manuscripts have been fully peer reviewed, but should not be considered the official version of record. They are citable by the Digital Object Identifier (DOI®). “Just Accepted” is an optional service offered to authors. Therefore, the “Just Accepted” Web site may not include all articles that will be published in the journal. After a manuscript is technically edited and formatted, it will be removed from the “Just Accepted” Web site and published as an ASAP article. Note that technical editing may introduce minor changes to the manuscript text and/or graphics which could affect content, and all legal disclaimers and ethical guidelines that apply to the journal pertain. ACS cannot be held responsible for errors or consequences arising from the use of information contained in these “Just Accepted” manuscripts.

Manipulating Topological Domain Boundaries in the Single-Layer Quantum Spin Hall Insulator $1T'-WSe_2$

Zahra Pedramrazi^{1†}, Charlotte Herbig^{1†}, Artem Pulkin^{2,3†}, Shujie Tang^{4,5,6}, Madeleine Phillips^{7,8}, Dillon Wong¹, Hyejin Ryu^{4,9}, Michele Pizzochero², Yi Chen¹, Feng Wang^{1,10,11}, Eugene J. Mele⁷, Zhi-Xun Shen^{5,6}, Sung-Kwan Mo⁴, Oleg V. Yazyev^{2,12}, Michael F. Crommie^{1,10,11*}

¹Department of Physics, University of California at Berkeley, Berkeley, CA 94720, USA.

²Institute of Physics, Ecole Polytechnique Fédérale de Lausanne (EPFL), CH-1015 Lausanne, Switzerland.

³Division of Chemistry and Chemical Engineering, California Institute of Technology, Pasadena, CA 91125, USA.

⁴Advanced Light Source, Lawrence Berkeley National Laboratory, Berkeley, CA 94720, USA.

⁵Stanford Institute for Materials and Energy Sciences, SLAC National Accelerator Laboratory, Menlo Park, CA 94025, USA.

⁶Geballe Laboratory for Advanced Materials, Departments of Physics and Applied Physics, Stanford University, Stanford, CA 94305, USA.

⁷Department of Physics and Astronomy, University of Pennsylvania, Philadelphia, PA 19104, USA.

⁸Center for Computational Materials Science, Naval Research Laboratory, Washington, D.C. 20375, USA.

⁹Center for Spintronics, Korea Institute of Science and Technology, Seoul 02792, Korea.

¹⁰Materials Sciences Division, Lawrence Berkeley National Laboratory, Berkeley, CA 94720, USA.

¹¹Kavli Energy NanoScience Institute at the University of California Berkeley and the Lawrence Berkeley National Laboratory, Berkeley, CA 94720, USA.

¹²National Centre for Computational Design and Discovery of Novel Materials MARVEL, Ecole Polytechnique Fédérale de Lausanne (EPFL), CH-1015 Lausanne, Switzerland.

† These authors contributed equally to this work.

*e-mail: crommie@berkeley.edu

Abstract

We report the creation and manipulation of structural phase boundaries in the single-layer quantum spin Hall insulator $1T'-WSe_2$ by means of scanning tunneling microscope tip pulses.

We observe the formation of one-dimensional interfaces between topologically non-trivial $1T'$ domains having different rotational orientations, as well as induced interfaces between

1
2
3 topologically non-trivial 1T' and topologically trivial 1H phases. Scanning tunneling
4 spectroscopy measurements show that 1T'/1T' interface states are localized at domain
5 boundaries, consistent with theoretically predicted unprotected interface modes that form
6 dispersive bands in and around the energy gap of this quantum spin Hall insulator. We observe a
7 qualitative difference in the experimental spectral lineshape between topologically “unprotected”
8 states at 1T'/1T' domain boundaries and protected states at 1T'/1H and 1T'/vacuum boundaries
9 in single-layer WSe₂.
10
11
12
13
14
15
16
17
18
19
20

21 Keywords: Scanning tunneling microscopy, transition metal dichalcogenides, quantum spin hall
22 insulators, domain boundary, ferroelasticity.
23
24
25
26
27

28
29 Recent experimental studies have reported the observation of the quantum spin Hall (QSH)
30 effect in single layers of the transition metal dichalcogenides (TMDs) WTe₂ and WSe₂ in the 1T'
31 structural phase.¹⁻⁵ Evidence of the QSH state include inverted bandgaps,¹ topologically
32 protected edge states,^{1,2,5} as well as quantized edge conduction of e^2/h per edge.^{3,4} QSH edge
33 states have been observed to reside at 1T'/1H and 1T'/vacuum boundaries, both of which are
34 interfaces between non-trivial (1T'–TMD) and trivial (1H–TMD phase or vacuum) media.^{1,2,5}
35 Such interfaces are expected to host topologically protected edge states.⁶⁻¹¹ A less well-studied
36 type of boundary in quantum spin Hall insulator (QSHI) materials is the interface between
37 different non-trivial domains where the Z_2 topological invariant of the bulk does *not* change
38 across the interface. We refer to a domain boundary as “topological” when there is a change in
39 the topological invariant across the interface, and “trivial” when the invariant is the same on
40 either side of the domain wall. A recent theoretical study of charge transport in quantum Hall
41
42
43
44
45
46
47
48
49
50
51
52
53
54
55
56
57
58
59
60

1
2
3 insulators with trivial interfaces predicted that conduction through otherwise dissipationless
4 quantum Hall edge states can be controllably deflected into trivial interface states, thus enabling
5 gate-tunable charge and spin transport.¹² Single-layer TMD materials provide a new strategy for
6 constructing such coexisting topological and trivial interfaces by switching the layer structural
7 phase via some local stimuli.¹³⁻¹⁷ For example, the 1T' phase has recently been predicted to be
8 ferroelastic in single layers, suggesting that it can be switched between different dimerization
9 orientations by applied stress. This provides a mechanism to induce topologically trivial
10 interfaces between QSHI domains with different crystallographic orientations. A similar strategy
11 could allow generation of topologically non-trivial interfaces by inducing local phase switching
12 between structures that have different Z_2 indices.^{18,19}

13
14
15
16
17
18
19
20
21
22
23
24
25
26 Here we report the local phase manipulation of single-layer 1T'-WSe₂ for the purpose of
27 creating two kinds of one-dimensional interfaces: (1) trivial interfaces between two 1T' domains
28 and (2) topological interfaces between 1T' and 1H domains. By using scanning tunneling
29 microscope (STM) tip pulses we are able to locally switch from the 1T' phase to the 1H phase of
30 WSe₂, as well as between different orientations of the 1T' phase. 1T'/1T' domain-boundary
31 formation is observed to be reversible, supporting the conjecture that single-layer 1T'-WSe₂ is a
32 ferroelastic material.¹⁸ Our STM measurements show that 1T'/1T' domain boundaries are well-
33 ordered interfaces that exhibit several different structures. By combining scanning tunneling
34 spectroscopy (STS) measurements and first-principles calculations we have determined that
35 1T'/1T' domain boundaries exhibit topologically unprotected one-dimensional (1D) modes that
36 are dispersive near the Fermi level and that exhibit energy dependent decay lengths. These
37 modes reside both inside and outside of the 1T'-bulk bandgap and, unlike 1T'/1H interface
38 modes, do not directly connect bulk valence and conduction bands.

Results

Mixed-phase single layers of WSe₂ were grown using molecular beam epitaxy (MBE) on bilayer graphene (BLG) supported by SiC. These samples exhibit islands that are single domains of either 1T' or 1H phase, as well as mixed-phase islands with coexisting 1T' and 1H domains.² Voltage pulses applied between the STM tip and monolayer 1T'–WSe₂ islands were used to manipulate the WSe₂ structural phase. Fig. 1 shows STM topographic images of a 1T'–WSe₂ island before and after application of STM tip pulses. The “before” image (Fig. 1a) shows a single-domain region of the 1T' phase with a uniform orientation of atomic rows running from top to bottom (each row contains a zigzag chain of W atoms^{1,2,9,11}). Fig. 1b shows the same region after a voltage pulse of 10 V was applied for 100 ms between the tip and surface at a constant tip-surface separation of ~6 Å. After application of the pulse the island exhibits multiple domains having different orientations that are connected by ordered 1D domain boundaries (tip pulses can also cause the formation of adsorbate clusters near domain boundaries, as shown in Fig. S7).

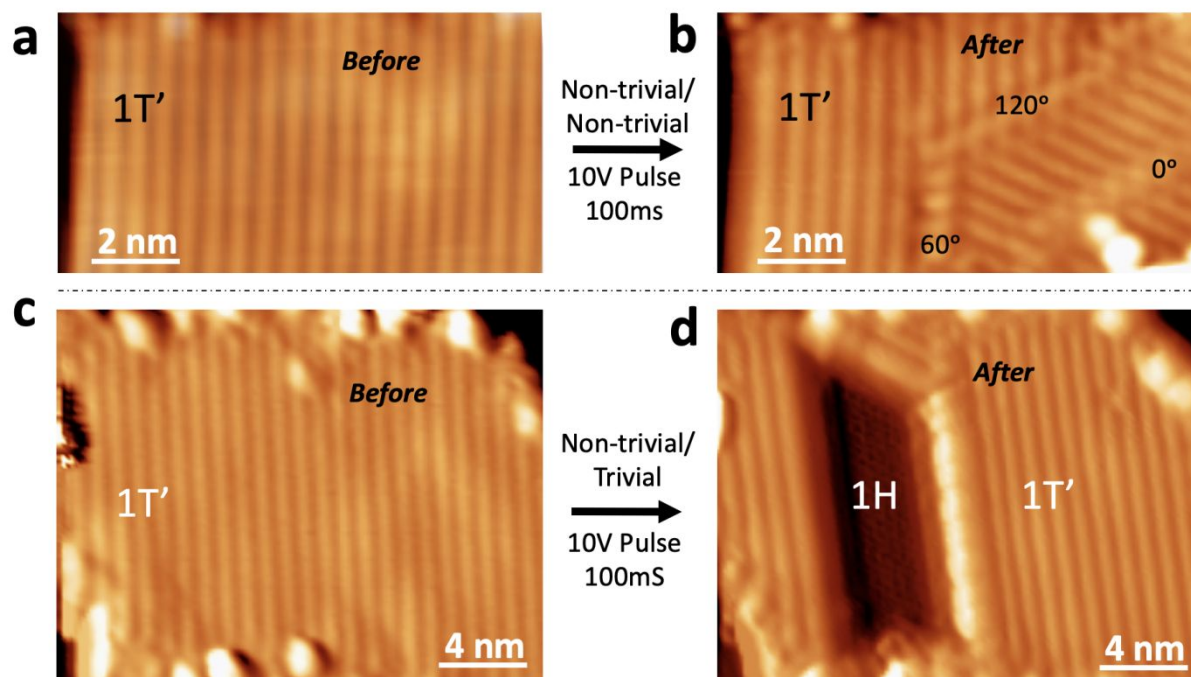


Figure 1: STM tip-induced structural change in monolayer 1T'–WSe₂. STM topographic images of a monolayer 1T'–WSe₂ island (a) before and (b) after applying a tip voltage pulse ($V_{\text{pulse}} = 10 \text{ V}$, $\Delta t = 100 \text{ ms}$, tip-surface separation = 6 \AA). The tip pulse creates 1T'/1T' domain boundaries having different rotational orientations. STM topographic images show a different island (c) before and (d) after an applied tip voltage pulse ($V_{\text{pulse}} = 10 \text{ V}$, $\Delta t = 100 \text{ ms}$, tip-surface separation = 6 \AA) induces a 1T' to 1H structural phase transition near the center of the island. $V_s = 1 \text{ V}$, $I_t = 10 \text{ pA}$, $T = 4.5 \text{ K}$ for all images. (Image intensity here is proportional to dz/dx (where z is height) in order to enhance contrast between regions having different structural phases.)

Because the 1T' phase can be formed in three equivalent orientations (via a Peierls distortion of its C_3 -symmetric 1T parent phase) several possible 1T'/1T' domain boundaries are expected.¹⁸ The most common 1T'/1T' interface observed in our samples is the 120° domain boundary which occurs for 85% of all observed boundaries and which connects neighboring

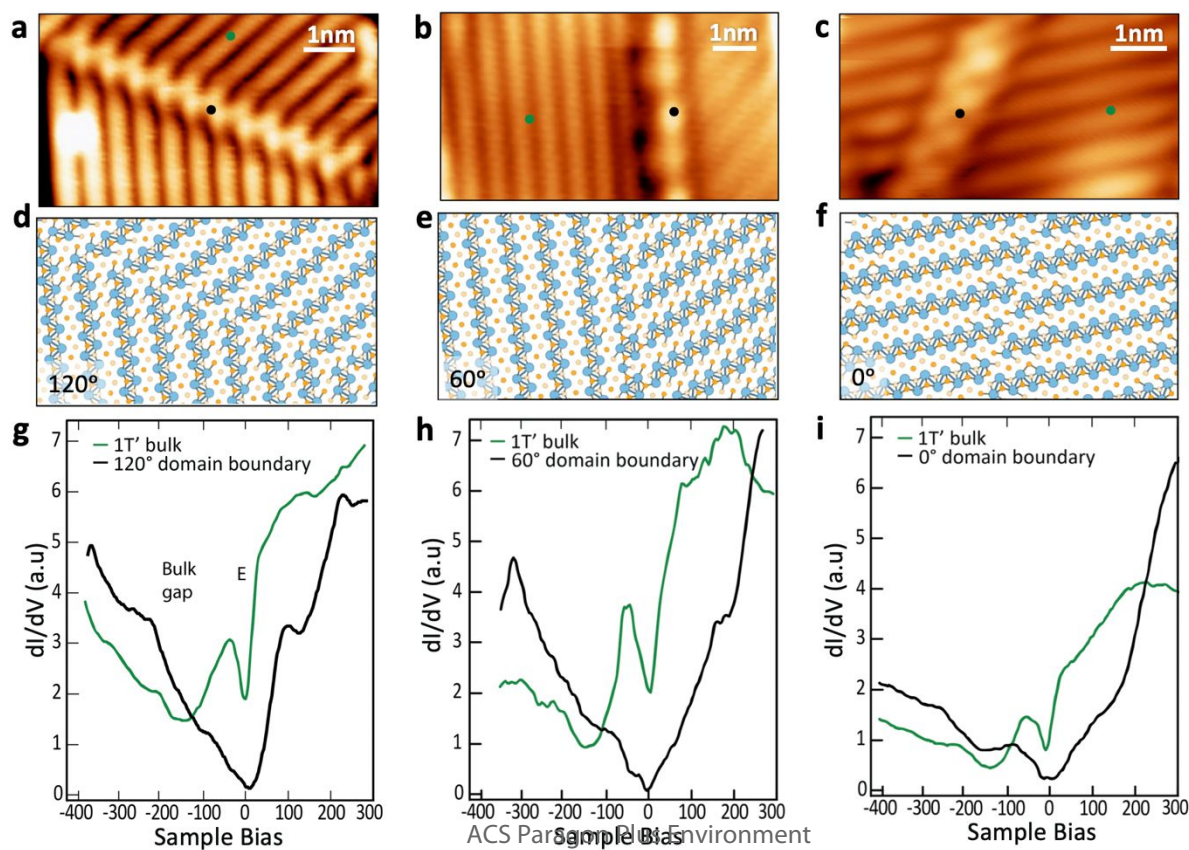
1
2
3 domains rotated with respect to each other by 120° (Fig. 2a). Other observed domain boundaries
4
5 are the 60° domain boundary (observed 13% of the time) and the 0° domain boundary (observed
6
7 2% of the time), as shown in Figs. 2b, c (structural models are shown in Figs. 2d-f). These well-
8
9 ordered interfaces are straight-line defects that extend up to 20 nm in length in our samples. The
10
11 formation of $1T'/1T'$ domain boundaries is reversible through the application of a high current
12
13 raster scan by the STM (300mV, 1nA). Such scans remove the adsorbate clusters that form
14
15 during the generation of $1T'/1T'$ domains, likely changing local strain distributions. This
16
17 provides additional evidence of the ferroelastic nature of $1T'$ - WSe_2 (further details are discussed
18
19 in section 6 of the SI).
20
21
22
23

24 The local conversion of single-layer WSe_2 from the $1T'$ phase to the 1H phase can be
25
26 induced using the same voltage pulse method as described above. Fig. 1c shows a different
27
28 single-phase $1T'$ island where the dimer chains run from top to bottom before applying a tip
29
30 pulse, while Fig. 1d shows the same region after applying a voltage pulse of 10 V for 100 ms.
31
32 The tip pulse causes an extended region of the island to convert into a new phase that exhibits
33
34 reduced apparent height. We identified this region as the 1H phase of single-layer WSe_2 (see Fig.
35
36 S6 for details). Such $1T'$ to 1H phase conversion was only observed in “confined” regions as
37
38 seen here (i.e. tip-induced 1H domains were always surrounded by other material).
39
40
41

42 While $1T'/1T'$ domain boundaries could be created by applying tip pulses with $V_{\text{pulse}} \geq 6$
43
44 V, stronger tip pulses ($V_{\text{pulse}} \geq 10$ V) were required to locally induce the $1T'$ to 1H phase
45
46 transition. These observations agree with predictions that the transition barrier between different
47
48 orientations of the $1T'$ phase should be lower than the barrier for a $1T' \rightarrow 1H$ transition.¹⁸ Tip
49
50 pulses with $V_{\text{pulse}} > 6$ V often caused damage to $1T'$ islands, either by creating holes or by
51
52
53
54
55
56
57
58
59
60

breaking apart the island. However, once $1T'/1T'$ and $1T'/1H$ domain structures are successfully induced then they remain stable under normal scan conditions.

In order to explore the electronic structure of topologically trivial interfaces in a QSHI we performed STS at the sites of the 120° , 60° , and 0° boundary structures shown in Figs. 2a-c. The dI/dV spectra obtained in the $1T'$ bulk (green curves in Figs. 2g-i) reflect the $1T'$ - WSe_2 bulk bandgap which has an average full width at half maximum (FWHM) of 85 ± 21 mV centered at -130 ± 5 mV (determination of the bulk bandgap was performed as described in Supplementary Note 3 of ref. 2). The spectral weight observed inside the bulk bandgap is explained by lifetime broadening and the -130 mV offset is due to n-doping induced by the bilayer graphene/SiC substrate, consistent with previous studies.^{2,20,21} The narrow dip at $V=0$ seen in Figs. 2g-i likely arises from an interplay between disorder and long-range electron-electron interactions as has been suggested previously.^{2,5,20,21,27,28} This feature is more pronounced at 1D domain boundaries which is consistent with predictions regarding disorder-induced behavior in low dimensions.²⁸



1
2
3
4 **Figure 2: Structural and electronic properties of 1T'/1T' domain boundaries.** STM images
5 of (a) 120°, (b) 60°, and (c) 0° 1T'/1T' domain boundaries in 1T'-WSe₂ ($V_s = 1$ V, $I_t = 10$ pA,
6 standard STM topographs). Relaxed structural models of (d) 120°, (e) 60°, and (f) 0° domain
7 boundaries in 1T'-WSe₂ (calculated using DFT). STM dI/dV spectroscopy measured at (g)
8 120°, (h) 60°, and (i) 0° domain boundaries compared to the bulk for single-layer 1T'-WSe₂
9 (spectroscopy positions marked by black and green dots in (a)-(c)) ($f = 613.7$ Hz, $V_{ac} = 4$ mV, $T =$
10 4.5 K. Initial tunneling parameters for spectroscopy measurements: $V_s = -400$ mV, $I = 100$ pA).
11
12
13
14
15
16
17
18
19
20
21
22

23 The spectra for the 120° and 60° domain boundaries (Figs. 2g, h) are similar in that they
24 both have a minimum at $V = 0$ and exhibit broad, sloping features in the filled state regime over
25 the range -300 mV $< V_s < 0$. Neither of these domain boundaries show any significant signatures
26 of the bulk bandgap. The 0° domain boundary (Fig. 2i) also has a minimum at $V = 0$, but it
27 shows a pronounced dip right in the bulk bandgap energy range. These experimental features are
28 qualitatively different from dI/dV spectra observed at topologically-protected 1T'/vacuum and
29 1T'/1H boundaries where a clearly defined edge-state peak is seen at the bulk bandgap energy² (a
30 reference dI/dV spectrum taken at the topological 1T'/vacuum edge is shown in Fig. S8).
31
32
33
34
35
36
37
38
39
40

41 Because the 120° domain boundaries are the dominant defect feature, we performed a more
42 in-depth study of their spatially-dependent electronic structure. Fig. 3 shows dI/dV maps over the
43 energy range -400 mV $< V_s < 150$ mV for a 120° 1T'/1T' domain boundary that intersects a
44 1T'/1H domain boundary. The first panel (Fig. 3a) shows an STM topograph of the region and
45 includes the 120° 1T'/1T' domain boundary (dashed oval) as well as the 1T'/1H boundary
46 (marked by a vertical dashed line with the 1T' phase to the right). This area allows us to
47
48
49
50
51
52
53
54
55
56
57
58
59
60

simultaneously compare the electronic structure of “topological” and “trivial” domain boundaries.

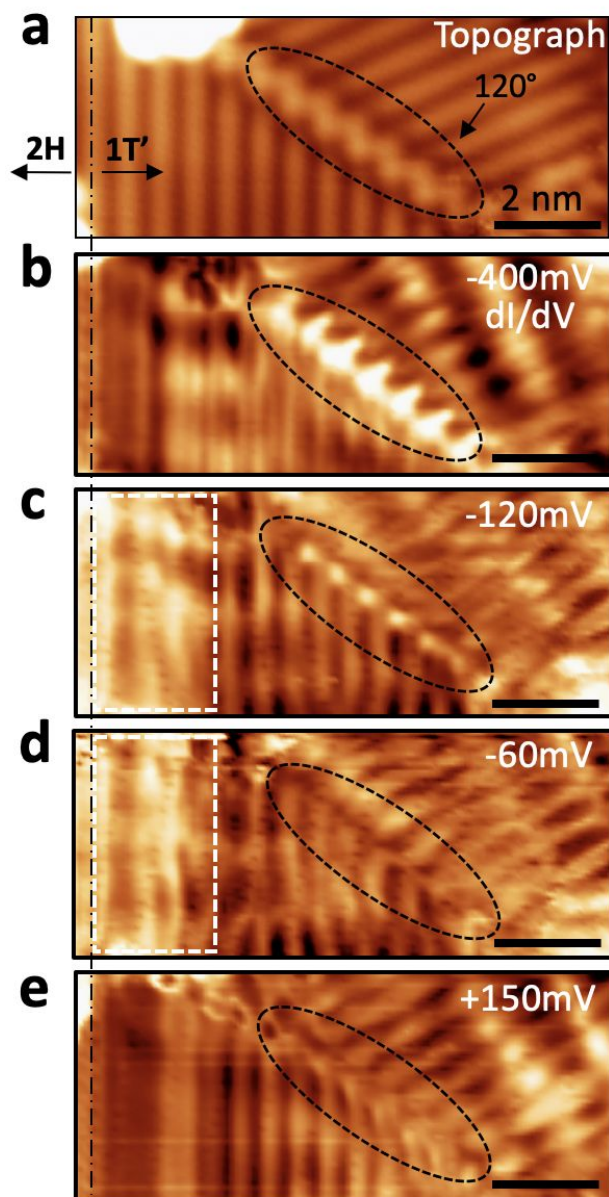


Figure 3: Comparison of electronic properties of 120° 1T'/1T' domain boundary and 1T'/1H boundary coexisting in single-layer WSe₂. (a) STM image of a mixed-phase WSe₂ island with a 120° 1T'/1T' domain boundary (standard STM topograph). The 1T'/1H interface is marked by a vertical dashed line while the 1T'/1T' interface is outlined by a dashed oval ($V_s = 1$ V, $I_t = 10$ pA). dI/dV maps of the same area are shown for (b) $V_s = -400$ mV, (c) -120 mV, (d) $-$

1
2
3 60 mV, and (e) +150 mV. Spectroscopy parameters: $f = 613.7$ Hz, $V_{ac} = 4$ mV, $I = 100$ pA, $T =$
4
5 4.5 K. Dashed white box outlines the topologically protected edge-state.

6
7
8 Fig. 3b shows a dI/dV map measured at -400 mV, which corresponds to an energy below
9
10 the lower edge of the bulk $1T'-WSe_2$ bandgap shown in Fig. 2g (i.e., the bulk valence states).
11
12 Bright intensity corresponding to high LDOS is observed at the site of the 120° domain boundary
13
14 while the LDOS near the $1T'/1H$ interface remains low. Fig. 3c shows a dI/dV map at -120 mV,
15
16 which lies inside the $1T'$ bulk bandgap. At this energy high LDOS intensity is observed at both
17
18 the 120° domain boundary and the $1T'/1H$ interface region (intensity near the $1T'/1H$ boundary
19
20 originates from the topological edge state.² Fig. 3d shows a dI/dV map measured at -60 mV,
21
22 which is near the upper edge of the bulk bandgap. Here high-intensity LDOS is observed near
23
24 the $1T'/1H$ interface (from the topological edge state), while the LDOS at the 120° domain
25
26 boundary shows low intensity. Fig. 3e shows a dI/dV map measured at $+150$ mV, which
27
28 corresponds to an energy well into the bulk conduction band. At this energy neither the
29
30 topological $1T'/1H$ interface state nor the trivial 120° domain boundary show high intensity
31
32 features. The high intensity LDOS localized at the $1T'/1T'$ boundary in the dI/dV maps indicates
33
34 the existence of defect states in the energy range -400 mV $< V_s < -60$ mV. The broad
35
36 spectroscopic feature measured in the dI/dV point spectrum over this range for 120° domain
37
38 boundaries (Fig. 2g) can thus be attributed to confined dispersive defect modes. The 120°
39
40 domain boundary mode is seen to have a more strongly energy-dependent decay length than the
41
42 $1T'/1H$ interface state and to have more intensity at lower energies.
43
44
45
46
47
48

49
50 In order to clarify the origin of these electronic features, we performed first-principles DFT
51
52 simulations. The atomic structure of the interfaces was first relaxed using periodic boundary
53
54 conditions in a ribbon geometry with a plane-wave basis set²² (the relaxed structures are
55
56
57
58
59
60

1
2
3 presented in Figs. 2d-f). We then used the non-equilibrium Green's function method (NEGF) to
4 model the line defects with semi-infinite boundary conditions.^{23,24} The resulting spin-dependent
5 electronic band structures for the three different interfaces are presented in Figs. 4a-c. The
6 number of bands, the dispersion, and the spin character of the defect modes changes dramatically
7 for the different boundary types. Defect modes belonging to the 60° domain boundary (which
8 has the least amount of symmetry) span the entire bandgap energy region while the localized
9 states of the 120° and 0° domain boundaries do not completely close the bulk energy gap (the
10 bulk bandgap of the 60° domain boundary model is somewhat affected by the strain that arises
11 from matching bulk lattice constants with the defect periodicity). We see that while the defect
12 modes mostly close the overall energy gap for the 60° and 120° domain boundaries, the gap
13 remains bulk-like for the 0° defect, consistent with our STM spectroscopy observations (Figs.
14 2g-i). The simulated 120° domain boundary states are observed to be spin-polarized out of the
15 plane while for 60° domain boundaries the direction of spin polarization rotates for different
16 states within the same band (colors in Figs. 4a, b). 0° domain boundaries possess inversion
17 symmetry and so defect states associated with this boundary show no spin polarization (Fig. 4c).
18
19
20
21
22
23
24
25
26
27
28
29
30
31
32
33
34
35
36
37
38
39
40
41
42
43
44
45
46
47
48
49
50
51
52
53
54
55
56
57
58
59
60

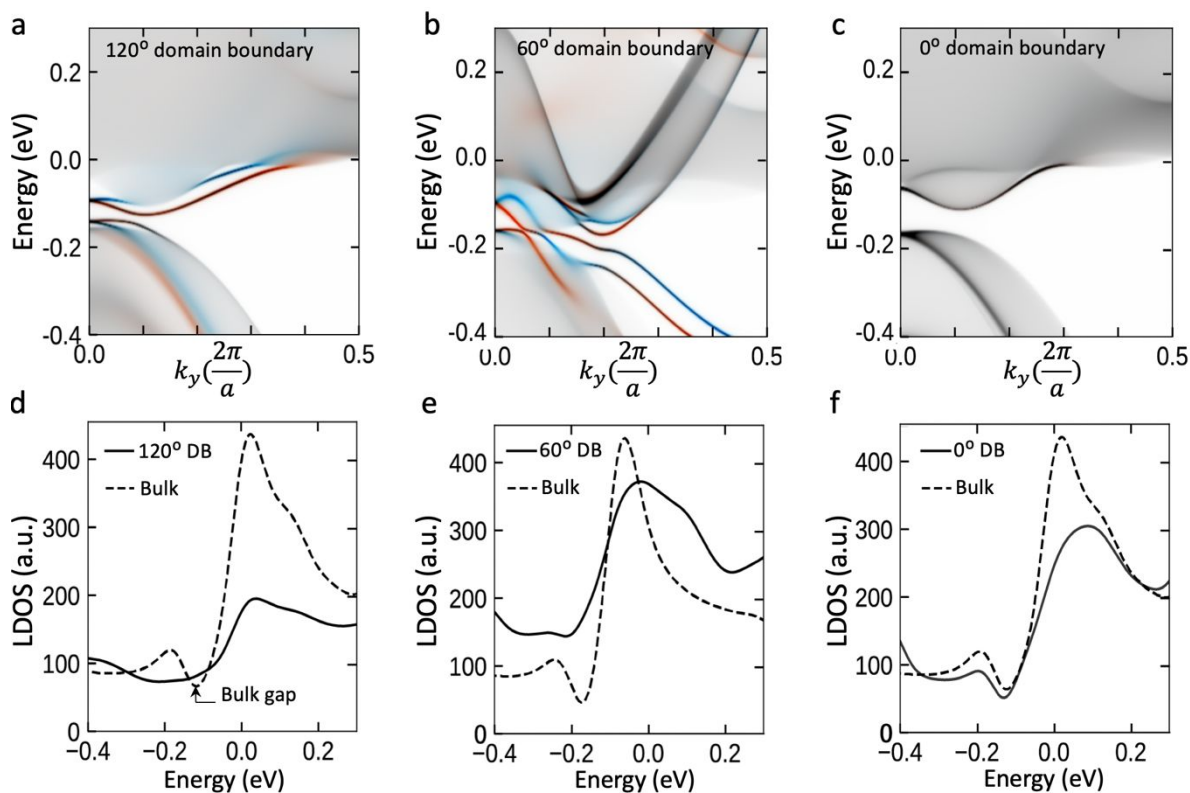


Figure 4: Calculated Band Structure and Local Density of States of Different 1T'/1T' Domain Boundaries.

Calculated band structure of (a) 120°, (b) 60°, and (c) 0° 1T'/1T' domain boundaries for 1T'-WSe₂ monolayer. Bulk states are grey, spin-polarized interface modes are red and blue. (d-f) Calculated LDOS of top-layer Se atoms at a domain boundary (black solid curve) compared to LDOS in the bulk (black dashed curve) for (d) 120°, (e) 60°, and (f) 0° 1T'/1T' domain boundaries. The Fermi level ($E = 0$) has been shifted to match experimental data (plots presented in (d)-(f) have been convolved with a Gaussian having $\sigma = 30$ mV to simulate level broadening effects²⁵).

Figs. 4d-f compare the calculated LDOS of the 120°, 60° and 0° domain boundaries (blue curves) with the LDOS of the 1T' bulk (grey curves) as a function of energy (the Fermi level has been shifted to match the experimentally observed n-doping). Overall we find reasonable agreement between the simulated LDOS in Fig. 4 and the corresponding STM spectroscopy

1
2
3 measurements of Fig. 2. For example, while the experimental bulk bandgap feature vanishes for
4
5 the 60° defect (Fig. 2h), an energy gap remains for the 0° defect (Fig. 2i), similar to the theory
6
7 plots of Figs. 4e, f. In the 120° case the predicted small 10 meV energy gap is likely smeared out
8
9 by level broadening effects that are observed experimentally but not accounted for in
10
11 conventional DFT simulations.²⁵ When we add Gaussian broadening to our calculation then the
12
13 120° gap feature is smeared out (Fig. 4d) similar to what is seen experimentally (Fig. 2g). A
14
15 significant discrepancy between the theory and the data is the pronounced LDOS peak seen near
16
17 $E = 0$ for all three domain boundary types. By contrast, all three domain boundaries show a
18
19 broad dip at $V = 0$ in the STM spectroscopy rather than the predicted peak. This is explained by
20
21 the coexistence of disorder and electron-electron interactions in these materials which opens a
22
23 pseudogap at $V = 0$ eV but which is not accounted for in DFT simulations.

28 **Conclusion**

29
30
31 In conclusion, we have successfully manipulated the local electronic and structural
32
33 properties of single-layer 1T'-WSe₂, thereby inducing a local phase transition from the 1T' to
34
35 the 1H phase, as well as creating 1T'/1T' domain boundaries. The induced 1T'/1T' domain
36
37 boundaries exhibit different rotational configurations, with a 120° domain boundary being the
38
39 most common structure. Our combined STS measurements and first-principles calculations show
40
41 that these new 1T'/1T' domain boundaries yield topologically unprotected 1D states that are
42
43 dispersive in energy near the Fermi level and exhibit energy-dependent decay lengths. These
44
45 results create new opportunities for exploring electron- and spin-based devices where charge
46
47 carriers traveling along QSH edges might be deflected into trivial domain boundary modes in a
48
49 controllable fashion.¹²
50
51
52
53
54
55
56
57
58
59
60

ACKNOWLEDGEMENT

This research was supported as part of the Center for Novel Pathways to Quantum Coherence in Materials, an Energy Frontier Research Center funded by the U.S. Department of Energy, Office of Science, Basic Energy Sciences (STM spectroscopy and dI/dV mapping). Support was also provided by the National Science Foundation under award EFMA-1542741 (surface preparation and topographic characterization). The work performed at the ALS (film characterization) was supported by the Office of Basic Energy Sciences, US DOE under Contract No. DE-AC02-05CH11231. C. H. acknowledges the support of Alexander von Humboldt Foundation for a Feodor Lynen research fellowship. The work performed at the Stanford Institute for Materials and Energy Sciences and Stanford University (MBE growth) was supported by the Division of Materials Science, Office of Basic Energy Sciences, US DOE under contract No. DE-AC02-76SF00515. Theoretical modeling of the two-channel conductance by M.P. and E.J.M. was supported by the DOE Office of Basic Energy Sciences under grant DE-FG02-ER45118. M.P. acknowledges support from an NRC Research Associateship award at the U.S. Naval Research Laboratory. S. T. acknowledges the support from the CPSF-CAS Joint Foundation for Excellent Postdoctoral Fellows. H. R. acknowledges fellowship support from NRF, Korea through Max Planck Korea/POSTECH Research Initiative No. 2016K1A4A4A01922028. A.P., M.P., and O.V.Y. acknowledge support by the ERC Starting grant “TopoMat” (Grant No. 306504) (ab initio theoretical formalism development), as well as Swiss National Science Foundation grants No. 162612 (2D bulk electronic structure) and No. 172543 (1D interface electronic structure). First-principles calculations were performed at the Swiss National Supercomputing Centre (CSCS) under project s832 and the facilities of Scientific

1
2
3 IT and Application Support Center of EPFL. We thank Quansheng Wu for assistance with
4
5 calculations, and we want to thank Canxun Zhang with helpful discussion.
6
7

8
9 **Supporting Information Available:**

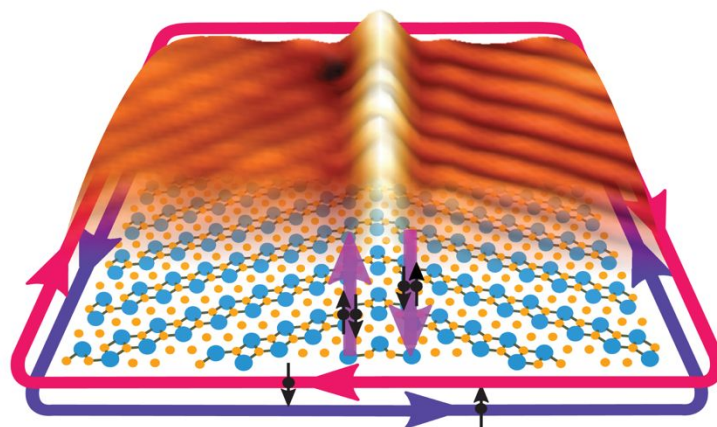
10
11 The SI contains detailed position-dependent spectroscopic measurements near a 0° and
12
13 120° domain boundary, dI/dV measurements of the topological edge state as well as dI/dV maps
14
15 of a 120° domain boundary. Further, theoretical calculations on the domain boundary structures,
16
17 the electronic structure of the $1T'$ -vacuum termination and LDOS of the three $1T'/1T'$ domain
18
19 boundaries plotted with different Gaussian smearing values are presented. A representative
20
21 illustration describing electronic behaviors (trivial versus non-trivial) of different possible
22
23 interface state as well as an example of a trivial/topological two-channel system are presented.
24
25 Experimental evidence for the ferroelasticity and further experimental detail on the tip-induced
26
27 $1H$ domain is provided. Theoretical and experimental analysis of the decay length for 120°
28
29 domain boundary states are given.
30
31
32
33
34

35 This material is available free of charge via the Internet at <http://pubs.acs.org>.
36
37
38
39
40
41
42
43
44
45
46
47
48
49
50
51
52
53
54
55
56
57

REFERENCES

- 1 Tang, S.; Zhang, C.; Wong, D.; Pedramrazi, Z.; Tsai, H. Z.; Jia, C.; Moritz, B.; Claassen, M.; Ryu, H.; Kahn, et al. Quantum Spin Hall State in Monolayer 1T'-WTe₂. *Nature Physics* **2007**, 13, 683-687.
- 2 Ugeda, M. M.; Pulkin, A.; Tang, S.; Ryu, H.; Wu, Q.; Zhang, Y.; Wong, D.; Pedramrazi, Z.; Martín-Recio, A.; Chen, Y.; et al. Observation of Topologically Protected States at Crystalline Phase Boundaries in Single-Layer WSe₂. *Nature Communications* **2018**, 9, 3401.
- 3 Wu, S.; Fatemi, V.; Gibson, Q. D.; Watanabe, K.; Taniguchi, T.; Cava, R. J.; Jarillo-Herrero, P. Observation of the Quantum Spin Hall Effect up to 100 Kelvin in a Monolayer Crystal. *Science* **2018**, 359, 76-79.
- 4 Fei, Z.; Palomaki, T.; Wu, S.; Zhao, W.; Cai, X.; Sun, B.; Nguyen, P.; Finney, J.; Xu, X.; Cobden, D. Edge Conduction in Monolayer WTe₂. *Nature Physics* **2017**, 13, 677-682.
- 5 Jia, Z.-Y.; Song, Y.-H.; Li, X.-B.; Ran, K.; Lu, P.; Zheng, H.-J.; Zhu, X.-Y.; Shi, Z.-Q.; Sun, J.; Wen, J.; et al. Direct Visualization of a Two-Dimensional Topological Insulator in the Single-Layer 1T'-WTe₂. *Physical Review B* **2017**, 96, 041108(R).
- 6 Kane, C. L.; Mele, E. J. Quantum Spin Hall Effect in Graphene. *Physical Review Letters* **2015**, 95, 226801.
- 7 Bernevig, B. A.; Zhang, S.-C. Quantum Spin Hall Effect. *Physical Review Letters* **2006**, 96, 106802.
- 8 Hasan, M. Z.; Kane, C. L. Colloquium: Topological Insulators. *Reviews of Modern Physics* **2010**, 82, 3045.
- 9 Qian, X.; Liu, J.; Fu, L.; Li, J. Quantum Spin Hall Effect in Two-Dimensional Transition Metal Dichalcogenides. *Science* **2014**, 346, 1344-1347.
- 10 Ma, Y.; Kou, L.; Li, X.; Dai, Y.; Smith, S. C.; Heine, T. Quantum Spin Hall Effect and Topological Phase Transition in Two-Dimensional Square Transition-Metal Dichalcogenides. *Physical Review B* **2015**, 92, 085427.
- 11 Choe, D.-H.; Sung, H.-J.; Chang, K. J. Understanding Topological Phase Transition in Monolayer Transition Metal Dichalcogenides. *Physical Review B* **2016**, 93, 125109.
- 12 Phillips, M.; Mele, E. J. Charge and Spin Transport on Graphene Grain Boundaries in a Quantizing Magnetic Field. *Physical Review B* **2017**, 96, 041403.
- 13 Wang, Y.; Xiao, J.; Zhu, H.; Li, Y.; Alsaied, Y.; Fong, K. Y.; Zhou, Y.; Wang, S.; Shi, W.; Wang, Y.; et al. Structural Phase Transition in Monolayer MoTe₂ Driven by Electrostatic Doping. *Nature* **2017**, 550, 487-491.
- 14 Lin, Y.-C.; Dumcenco, D. O.; Huang, Y.-S.; Suenaga, K. Atomic Mechanism of the Semiconducting-to-Metallic Phase Transition in Single-Layered MoS₂. *Nature Nanotechnology* **2014**, 9, 391-396.
- 15 Keum, D. H.; Cho, S.; Kim, J. H.; Choe, D.-H.; Sung, H.-J.; Kan, M.; Kang, H.; Hwang, J.-Y.; Kim, S. W.; Yang, H.; et al. Bandgap Opening in Few-Layered Monoclinic MoTe₂. *Nature Physics* **2015**, 11, 482-486.

- 1
2
3 16 Kappera, R.; Voiry, D.; Yalcin, S. E.; Branch, B.; Gupta, G.; Mohite, A. D.; Chhowalla,
4 M. Phase-engineered Low-Resistance Contacts for Ultrathin MoS₂ Transistors. *Nature*
5 *Materials* **2014**, 13, 1128-1134.
6
7 17 Li, Y.; Duerloo, K.-A. N.; Wauson, K.; Reed, E. J. Structural Semiconductor-to-
8 Semimetal Phase Transition in Two-Dimensional Materials Induced by Electrostatic
9 Gating. *Nature Communications* **2016**, 7, 10671.
10
11 18 Li, W.; Li, J. Ferroelasticity and Domain Physics in Two-Dimensional Transition Metal
12 Dichalcogenide Monolayers. *Nature Communications* **2016**, 7, 10843.
13
14 19 Duerloo, K.-A. N.; Li, Y.; Reed, E. J. Structural Phase Transitions in Two-Dimensional
15 Mo- and W-Dichalcogenide Monolayers. *Nature Communications* **2014**, 5, 4214.
16
17 20 Song, Y.-H.; Jia, Z.-Y.; Zhang, D.; Zhu, X.-Y.; Shi, Z.-Q.; Wang, H.; Zhu, L.; Yuan, Q.-
18 Q.; Zhang, H.; Xing, D.-Y.; et al. Observation of Coulomb Gap in the Quantum Spin Hall
19 Candidate Single-Layer 1T'-WTe₂. *Nature Communications* **2018**, 9, 4071.
20
21 21 Massey, J. G.; Lee, M. Direct Observation of the Coulomb Correlation Gap in a
22 Nonmetallic Semiconductor, Si: B. *Physical Review Letters* **1995**, 75, 4266.
23
24 22 Giannozzi, P.; Baroni, S.; Bonini, N.; Calandra, M.; Car, R.; Cavazzoni, C.; Ceresoli, D.;
25 Chiarotti, G. L.; Cococcioni, M.; Dabo, I.; et al. QUANTUM ESPRESSO: a Modular and
26 Open-Source Software Project for Quantum Simulations of Materials. *Journal of*
27 *Physics: Condensed Matter* **2009**, 201, 395502.
28
29 23 Ozaki, T. Variationally Optimized Atomic Orbitals for Large-Scale Electronic Structures.
30 *Physical Review B* **2003**, 67, 155108.
31
32 24 Ozaki, T.; Kino, H. Numerical Atomic Basis Orbitals from H to Kr. *Physical Review B*
33 **2004**, 69, 195113.
34
35 25 Brar, V. W.; Wickenburg, S.; Panlasigui, M.; Park, C.-H.; Wehling, T. O.; Zhang, Y.;
36 Decker, R.; Girit, Ç.; Balatsky, A. V.; Louie, S. G.; et al. Observation of Carrier-Density-
37 Dependent Many-Body Effects in Graphene via Tunneling Spectroscopy. *Physical*
38 *Review Letters* **2010**, 104, 036805.
39
40 26 Bychkov, Y. A.; Rashba, E. I. Properties of a 2D Electron Gas with a Lifted Spectrum
41 Degeneracy. *Phys. -JETP Lett.* **1984**, 39, 78-81.
42
43 27 Altshuler B. L.; Aronov, A. G. Zero Bias Anomaly in Tunnel Resistance and Electron-
44 Electron Interaction. *Solid State Commun.* **1979**, 30, 115-117.
45
46 28 Bartosch L.; Kopietz, P. Zero Bias Anomaly in the Density of States of Low-Dimensional
47 Metals. *Eur. Phys. J. B* **2002**, 28, 29-36.
48
49
50
51
52
53
54
55
56
57
58
59
60



For Table of Contents Only.

1
2
3
4
5
6
7
8
9
10
11
12
13
14
15
16
17
18
19
20
21
22
23
24
25
26
27
28
29
30
31
32
33
34
35
36
37
38
39
40
41
42
43
44
45
46
47
48
49
50
51
52
53
54
55
56
57
58
59
60

